Lellouch-Lüscher relation for ultracold few-atom systems under confinement

Jing-Lun Li, ^{1,2,*} Paul S. Julienne, ³ Johannes Hecker Denschlag, ¹ and José P. D'Incao^{4,†}

¹ Institut für Quantenmaterie and Center for Integrated Quantum

Science and Technology IQST, Universität Ulm, 89069 Ulm, Germany

² Institute of Science and Technology Austria (ISTA), Am Campus 1, 3400 Klosterneuburg, Austria

³ Joint Quantum Institute, University of Maryland,
and the National Institute of Standards and Technology (NIST), College Park, MD 20742, USA

⁴ Department of Physics, University of Massachusetts Boston, Boston, MA 02125, USA

(Dated: November 18, 2025)

We derive an analog of the Lellouch-Lüscher (LL) relation for few-body bosonic systems, linking few-body scattering loss rates to the energies and widths of the corresponding harmonically trapped few-body states. Three-body numerical simulations show that the LL relation applies across a broad range of interaction strengths and energies and allows the determination of scattering rates within a single partial wave. Our work establishes a robust theoretical framework for understanding the role of the finite volume effect in few-body observables in optical lattice and tweezer experiments, enabling precise determination of multi-body scattering rates.

Over the past few decades, trapped ultracold atoms and molecules have become a remarkably versatile platform for exploring and exploiting quantum phenomena, driving advances in atomic, molecular and optical physics, condensed matter, chemistry, and quantum information science and technology [1–9]. This success stems from the unparalleled level of control provided by ultracold atom systems over internal states, interatomic interactions, and trapping dynamics [10–13]. More recent advances in optical lattices and optical tweezers have further expanded the versatility of ultracold atoms by introducing deterministic control of the atom number (up to a few) in a single trap site [14–17]. These techniques enable novel approaches to quantum simulation [18] and allow deeper insight into the fundamental processes governing chemical reactions [19–21]. Furthermore, they pave the way for using trapped few-atom systems for quantum information applications, the exploration of multi-body interactions [22], and the study of many-body states created atom by atom [23].

In many ways, atoms and molecules trapped in optical lattices or tweezers form an ideal system for studying various fundamental aspects of few-body interactions. While in ultracold gas experiments few-body interactions are typically characterized by scattering loss rates, in trapped systems the key observables are the on-site interatomic interaction and the lifetime of individual trapped states [22–30]. Optical tweezers, in particular, have enabled the creation of fully isolated two- and three-atom systems that allow measurements of such physical observables at the single-event level [31–33]. While offering unprecedented control over few-body systems, such experiments also encounter two central challenges: how to relate measurements in confined setups to free-space scattering parameters and how confinement itself influences collision dynamics and system stability. Similar challenges arise in high-energy physics, particularly in lattice quantum chromodynamics, where calculations are performed in a finite volume. A major breakthrough in that context was the development of the well-known Lellouch-Lüscher (LL) relations [34–40], which provide a rigorous way to extract scattering observables -such as decay rates and cross sections- from the discrete energy levels of finite-volume simulations. The development of a similar approach for trapped few-atom systems has the potential to provide a more accurate and controllable procedure to determine few-atom scattering rates than in ultracold bulk gases. Isolated few-body systems allow for a clearer and more systematic way to distinguish scattering rates from processes involving varying numbers of atoms [33], a task that proves to be more challenging in bulk gases [41– 44]. Moreover, the ability of preparing trapped few-body states in well-defined quantum states [20, 22, 45-47] can enable the direct measurement of individual partial-wave scattering rates, providing a much more sensitive probe for resonance and interference effects often obscured by thermal effects in gases [48, 49].

In this Letter, we derive the analog of the LL relation for ultracold few-body systems trapped under harmonic confinement and provide numerical evidence of its validity. In particular, we consider a system of three identical bosons in an isotropic harmonic trap and focus on extracting the free-space energy-dependent three-body loss (recombination) rate coefficient, $L_3(E)$, characterizing the process where three free atoms collide at energy E to form a diatomic molecule. Our key finding is an LL relation that connects $L_3(E_q)$ at the energy $E_q > 0$ (q = 0, 1, 2, ...) of the q-th gas-like trapped three-body state in the lowest partial wave [50-52] to its corresponding width, Γ_q :

$$L_3(E_q) = C \frac{\hbar^4}{m^3} \frac{\Gamma_q}{\omega_{\text{ho}}[E_q^2 - (\hbar\omega_{\text{ho}})^2]}$$
 (1)

where m is the atomic mass, ω_{ho} the angular trap frequency and $C = 72\sqrt{3}\pi^3$, a universal constant. Conversely, if $L_3(E)$ is known, the LL relation predicts the

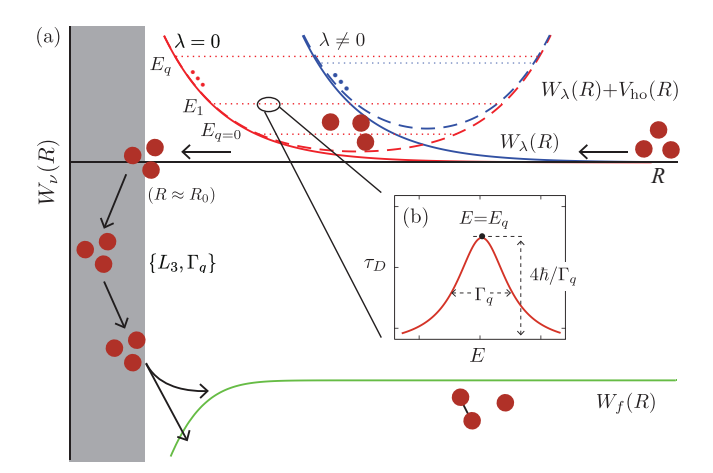


FIG. 1. (a) Schematic illustration of three-body losses in free space and in a harmonic trap. In free space, three atoms in continuum channels $W_{\lambda}(R)$ (solid) undergo inelastic transitions near $R \lesssim R_0$ (shaded) to atom-dimer channels $W_f(R)$, characterized by the recombination rate constant L_3 . In a trap, discrete states E_q (dotted) form in $W_{\lambda}(R) + V_{\text{ho}}(R)$ channels (dashed) and decay to atom-dimer channels with rate Γ_q/h [58]. (b) Trapped-state energies E_q and widths Γ_q manifest as Lorentzian resonances in the time delay $\tau_D(E)$ (see text).

lifetime, h/Γ_q , of the trapped three-body states [53]. We numerically verify our LL relation through simulations of ⁸⁵Rb and ⁸⁷Rb atoms using the hyperspherical adiabatic representation [54–56]. We show that the LL relation remains valid for states in which $a \ll r_{\rm ho}(q) \simeq (E_q/m\omega_{\rm ho}^2)^{1/2}$, where $r_{\rm ho}(q)$ is the characteristic size of the trap state and a is the two-body scattering length characterizing the strength of the interatomic interaction [10]. We generalize the LL relation to a system of N identical bosons opening up a path for the determination of multi-body scattering rates [22, 57]. These results provide a direct theoretical framework for interpreting few-body observables in optical lattices and tweezers experiments, where finite-volume effects play a central role.

In adiabatic hyperspherical representation [54, 55], after solving for the hyperangular motion, three-body observables are determined from the solutions of the hyperradial Schrödinger equation [54, 55]

$$\left[-\frac{\hbar^2}{2\mu} \frac{d^2}{dR^2} + W_{\nu}(R) - E \right] F_{\nu}(R) + \sum_{\nu' \neq \nu} W_{\nu\nu'}(R) F_{\nu'}(R) = 0,$$
 (2)

with adiabatic potentials W_{ν} and the non-adiabatic couplings $W_{\nu\nu'}$ obtained by solving adiabatic hyperangular equations at fixed values of the hyperradius R (see supplemental material [58] for more details). Here, ν is the set of quantum numbers necessary to characterize each channel, F_{ν} is the three-body hyperradial wave function, $\mu = m/\sqrt{3}$ the three-body reduced mass and m the atomic

mass. In Fig. 1(a) we show the adiabatic potentials W_{ν} for three-body loss in free space and in a harmonic trap. Here, $W_{\nu=\lambda}$ are continuum channels that describe the collision between three free atoms or, in a trap, support discrete three-body states. They are labeled by the hyperangular momentum $\lambda \geq 0 \in \mathbb{Z}$, which sets the hyperradial centrifugal barrier at large R [58]. (For bosonic systems the lowest value of λ is $\lambda_{\min} = 0$ while for fermionic systems $\lambda_{\min} \neq 0$ [59].) In Fig. 1(a), $W_{\nu=f}$ denotes an atom–dimer channel, which serves as the primary decay pathway leading to atomic losses.

The central physical quantities in the LL relation (1) can be extracted from the solutions of Eq. (2) in both free space and trapped systems. In free space, the rate constant for three-body recombination at collision energy E is defined as

$$L_3(E) = \sum_{J} \sum_{\lambda,f} 96\pi^2 \hbar \frac{(2J+1)}{\mu k^4} |S_{f\lambda}^J|^2 = \sum_{J} L_3^J(E), \quad (3)$$

with $k=(2\mu E/\hbar^2)^{1/2}$, f running over all final W_f (atom-dimer) channels, λ running over the initial (three-body continuum) W_{λ} channels, and the corresponding S-matrix obtained from the solutions of Eq. (2) [55]. In the above equation, L_3^J is the partial-wave contribution to L_3 for the total orbital angular momentum, J. For ultracold bosonic gases, the total rate $L_3(E)$ is dominated by the J=0 partial rate, with all other J contributions vanishing as $E\to 0$ [60, 61], only becoming important for energies beyond $E_c=\hbar^2/ma^2$ [48]. In the present work, we only study $L_3^{J=0}$ recombination and its connection to the lifetime of the J=0 trapped three-body states.

By introducing the harmonic trap $V_{\text{ho}}(R) = \mu \omega_{\text{ho}}^2 R^2/2$ into Eq. (2), each W_{λ} channel will support a series of trapped states with energy E_q and width Γ_q , arising from the decay into W_f channels (illustrated in Fig. 1(a); see further details in Ref. [58]).

Here, we focus only on trapped states associated with the $\lambda = \lambda_{\min} = 0$ channel, as this is also the dominant channel for $L_3(E)^{J=0}$ [55]. As we will see below, our numerical calculations shows that the with Γ_q for trapped states associated with $\lambda \neq 0$ are extremely narrow, as a result of the weak decay in such channels. (Note that in the following we omit J and λ in our notation unless stated otherwise.) Here, the energies and widths of the trap states are determined via the time delay,

$$\tau_D(E) \equiv 2\hbar \frac{d}{dE} \delta_S(E),$$
(4)

with the eigenphase-shift sum, δ_S , obtained from the corresponding S-matrix elements [62] extracted from the solutions of Eq. (2) with the trap $V_{\text{ho}}(R)$. As usual, near the energy of a trapped state, the time-delay exhibits a Lorentzian line shape [see Fig. 1(b)], reaching its maximum at $E = E_q$, with a corresponding width determined by $\Gamma_q = 4\hbar/\tau_D(E_q)$. See Ref. [58] for details on our numerical procedure to determine E_q and Γ_q .

After having introduced the theoretical framework for calculating numerically $L_3(E)$, E_q and Γ_q , we now present a simple analytical approach to derive the relationship between free-space and in-trap observables, i.e., the LL relation (1). Our derivation assumes weak interactions ($|a|/a_{\text{ho}} \ll 1$, where $a_{\text{ho}} = \hbar^{1/2}/(m\omega_{\text{ho}})^{1/2}$ is the oscillator length), but also weak trapping ($r_{\text{vdW}}/a_{\text{ho}} \ll 1$, with r_{vdW} being the van der Waals length [10, 58]). Our key observation is that the mechanism controlling both Γ_q and L_3 is identical, i.e., in both cases inelastic transitions occur primarily at short distances $R \leq R_0 \sim r_{\text{vdW}}$, as illustrated in Fig. 1(a). Accordingly, we define the following relation [62–64]:

$$\frac{\Gamma_q}{\hbar} = \frac{L_3(E_q)}{3} \mathcal{D}_q,\tag{5}$$

where the factor 3 accounts for the loss of three atoms per event, and \mathcal{D}_q is the reactive three-body probability defined the probability to find particles in the q-th state within the reaction region $(R \leq R_0)$, with hyperspherical volume $\mathcal{V}_0 = \pi^3 R_0^6/6$. In Ref. [58] we show that \mathcal{D}_q is closely related to the three-body correlation function [33]. In hyperspherical representation, \mathcal{D}_q is given by

$$\mathcal{D}_{q} = \frac{1}{\mathcal{V}_{0}} \int_{0}^{R_{0}} F_{q}(R)^{2} dR, \tag{6}$$

where F_q is the (non-interacting) hyperradial wavefunction for the q-th trapped three-body state [65] associated to the W_{λ} channel. For λ = 0, F_q is given by

$$F_q(R) = \frac{R^{5/2}}{N_q^{1/2} a_{\text{ho}}^3} L_q^{(2)} \left(\frac{R^2}{\sqrt{3} a_{\text{ho}}^2}\right) \exp\left(-\frac{R^2}{2\sqrt{3} a_{\text{ho}}^2}\right), \quad (7)$$

with energy $E_q = (2q+3)\hbar\omega_{\text{ho}}$. Here, $L_q^{(\alpha)}$ are the generalized Laguerre polynomials and $N_q = 3\sqrt{3}(q+1)(q+2)/2$ is a normalization constant. To leading order, the reactive probability density can be expressed as [58],

$$\mathcal{D}_q = \frac{m^3 \omega_{\text{ho}} (E_q^2 - \hbar^2 \omega_{\text{ho}}^2)}{24\pi^3 \sqrt{3} \hbar^5},\tag{8}$$

independent of the specific choice of R_0 . Substituting Eq. (8) into (5), we finally obtain the LL relation (1),

$$\Gamma_q = \frac{1}{C} \frac{m^3}{\hbar^4} L_3(E_q) [E_q^2 - (\hbar \omega_{\text{ho}})^2] \omega_{\text{ho}},$$
 (9)

with $C = 72\sqrt{3}\pi^3$. The above derivation of the bosonic J = 0 ($\lambda_{\min} = 0$) LL relation [Eqs. (1) and (9)] can be readily extended for to other bosonic and fermionic systems with arbitrary J (λ_{\min}) [59].

We note that beyond the weakly interacting regime $(|a|/a_{\text{ho}} \ll 1)$ trap effects are expect to alter the reaction process in non-trivial ways thus requiring modifications in \mathcal{D}_q resulting from the actual short-range

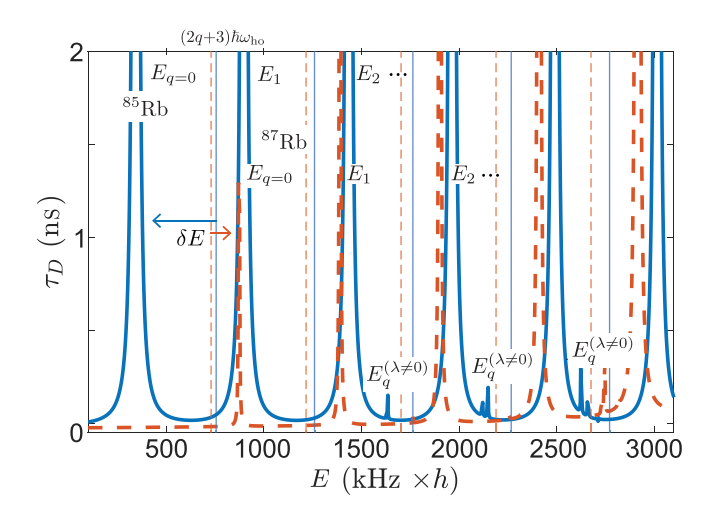


FIG. 2. A typical time delay plot for $^{85}{\rm Rb}$ at $\omega_{\rm ho}{=}2\pi{\times}252$ kHz or, equivalently, $|a|/a_{\rm ho}{=}1.11$ (solid line) and for $^{87}{\rm Rb}$ at $\omega_{\rm ho}{=}2\pi{\times}243$ kHz, or $|a|/a_{\rm ho}{=}0.24$ (dashed line). Both frequencies correspond to $a_{\rm ho}{=}5r_{\rm vdW}$. The vertical lines indicate the energy levels of three non-interacting atoms, $(2q+3)\hbar\omega_{\rm ho}$. Arrows indicate the shift $\delta E \propto a/a_{\rm ho}$ from the ground state energy $3\hbar\omega_{\rm ho}$ due to interactions. E_q denotes the energies for states of the $\lambda=0$ channel and $E_q^{(\lambda\neq0)}$ otherwise.

physics. However, we have found that for $|a|/a_{\rm ho} \simeq 1$ we can account for some of these effects by using the interacting energies E_q (obtained from our numerical calculations) in \mathcal{D}_q [Eq. (8)] and the LL-relation [Eqs. (1) and (9)]. In fact, for a specific state with E_q , the ratio $|a|/r_{\rm ho}(q)=(2q+3)^{-1/2}|a|/a_{\rm ho}\ll 1$ provides a more accurate measure the range of validity of the LL-relation than $|a|/a_{\rm ho}$, where $r_{\rm ho}(q)\simeq a_{\rm ho}(2q+3)^{1/2}\simeq (E_q/m\omega_{\rm ho}^2)^{1/2}$ characterize the state's size. Consequently, even when $|a|/a_{\rm ho}\simeq 1$, the LL relation will apply for highly excited trap states with $q\gg 1$.

We now test the validity of the LL relation through three-body numerical simulations of $^{85}\mathrm{Rb}$ and $^{87}\mathrm{Rb}$ atoms. Our numerical model employs reduced interatomic interaction potentials derived from Born-Oppenheimer potentials while incorporating the full atomic hyperfine spin structure [56, 66] (see also Ref. [58]). This interaction model encompasses more than 100 atom-dimer channels, with three-body potentials that span an energy range several thousands times larger than the characteristic vdW energy scale, $E_{\rm vdW}=\hbar^2/mr_{\rm vdW}^2$, below the three-body breakup threshold ($E\leq0$) [58].

The two isotopes of Rb atoms we use have vastly different physical properties: at zero-magnetic-field, the effective interaction between $^{85}{\rm Rb}$ atoms is strong and attractive, characterized by the large and negative value of $a=-5.56~r_{\rm vdW}$ while for $^{87}{\rm Rb}$ the effective interaction is weak and repulsive with $a=1.21~r_{\rm vdW}$ [58]. In the trap, the effect of the interaction strength manifests itself as a shift of the energy levels from their non-interacting val-

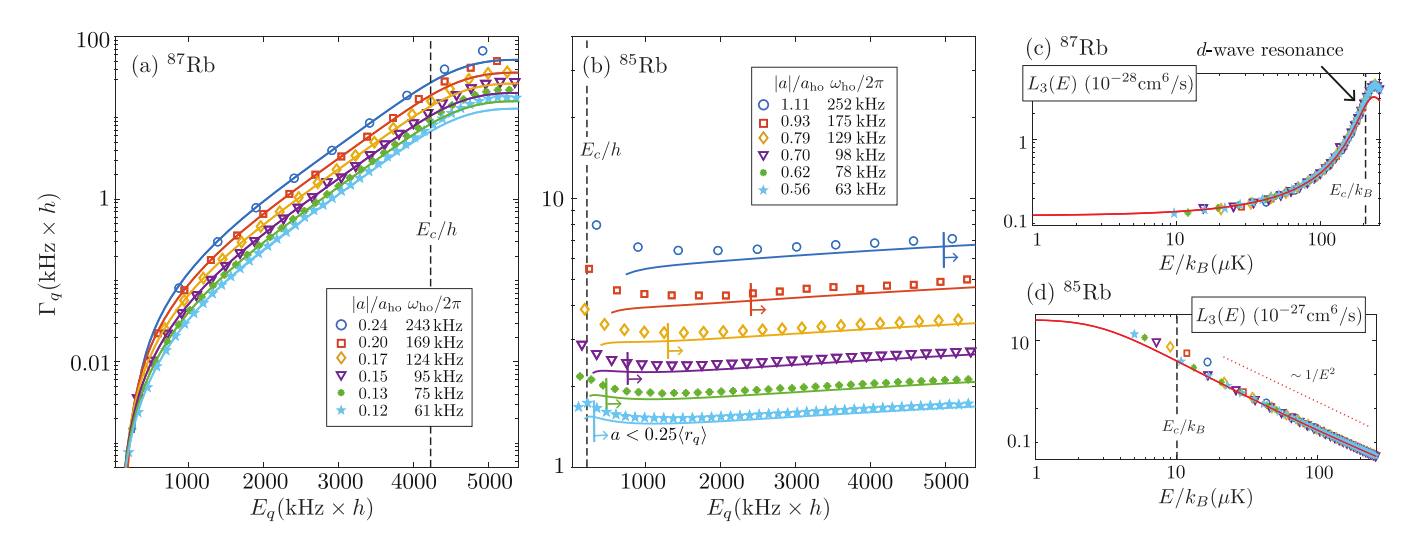


FIG. 3. Numerical values for the width Γ_q of the three-body states (symbols) as a function of their energy E_q for (a) ⁸⁷Rb, and (b) for ⁸⁵Rb. Solid lines correspond to the results for Γ_q from the LL relation (9), obtained from our free-space numerical simulations of $L_3(E)$. The colored arrows in (b) mark the regime $a < 0.25 \langle r_q \rangle$, and all data points in (a) fall within this regime. For both Rb isotopes the frequencies correspond to $a_{\rm ho}/r_{\rm vdW} = 5$, 6, 7, 8, 9 and 10. Symbols in (c) and (d) correspond to $L_3(E_q)$ from the LL relation (1) obtained from the numerical calculations for E_q and Γ_q shown in (a) and (b). The vertical dashed lines indicate the value of $E_c = \hbar^2/(ma^2)$.

ues, $(2q+3)\hbar\omega_{\text{ho}}$, with a leading-order shift $\delta E \propto a/a_{\text{ho}}$ [50]. This effect can be observed in Fig. 2 for the time delay for three ⁸⁵Rb (solid line) and ⁸⁷Rb (dashed line) atoms under strong confinement ($a_{\text{ho}} = 5 r_{\text{vdW}}$). Figure 2 shows $\lambda = 0$ trapped states for both atomic species manifested by the resonance feature (sudden increase) of the time-delay near $E = E_q$, shifted by δE from the noninteracting energies (vertical lines). Note that the narrow and unresolved features in Fig. 2 are associated with three-body trap states belonging to $\lambda \neq 0$ channels, highlighting their relative insignificance compared to the $\lambda = 0$ states [55]. More notably, while the resonances for ⁸⁵Rb are generally broad, with Γ_q largely insensitive to E_q , those for $^{87}\mathrm{Rb}$ display a clear transition from narrow to broad as E_q increases. In the following, we show that the LL relation provides a clear interpretation of these two distinct physical behaviors, attributed to the energy dependence of $L_3(E)$.

In Fig. 3, we validate our LL relation (9) by comparing the calculated Γ_q values (symbols) with LL predictions (solid lines), using our results for $L_3(E)$. Figure 3 presents results for trapping frequencies ranging from 60 kHz to 250 kHz, showing excellent agreement with the LL relation (9) in the regime $|a|/a_{\text{ho}} \ll 1$, with deviations emerging as $|a|/a_{\text{ho}}$ increases. For ⁸⁷Rb, since interactions are weak, all the values for $|a|/a_{\text{ho}}$ in Fig. 3(a) fall well within the $|a|/a_{\text{ho}} \ll 1$ regime the agreement with the LL relation (9) holds for all values of E_q , including those with energy comparable to $E_{\text{vdW}} \approx 6000 \text{ kHz} \times h$, therefore, beyond the ultracold regime $E_q \ll E_{\text{vdW}}$. For ⁸⁵Rb [Fig. 3(b)], however, due to its strong interactions, even at the lowest trap frequency, the ratio $|a|/a_{\text{ho}} (\approx 0.56)$ is

not deep in the $|a|/a_{\text{ho}} \ll 1$ regime, leading to a deviation from the LL relation for the lowest few E_q . For higher excited states, deviations become relatively small as E_q increases, confirming that the LL relation remains valid for $|a|/r_{\text{ho}}(q) \ll 1$, as noted previously.

Also evident in Figs. 3(a) and (b) is the contrasting behavior of Γ_q for ⁸⁷Rb and ⁸⁵Rb: for ⁸⁷Rb Γ_q is strongly dependent on E_q , while for ⁸⁵Rb it is relatively independent of E_q . According to the LL relation (9), this contrasting behavior can be understood as arising from the distinct energy dependence of L_3 for the two isotopes. For ⁸⁵Rb atoms, the primary factor influencing $L_3(E)$ results from its strong interactions (a = -5.56) $r_{\rm vdW}$). In such cases, the expected threshold behavior, $L_3(E) = \text{const}$, deteriorates for $E \gtrsim E_c = \hbar^2/(ma^2)$, with $L_3(E)$ reaching its unitary behavior, $L_3(E) = C_{\eta}/E^2$, where $C_{\eta} = 72\sqrt{3}\pi^2\hbar^5/m^3(1-e^{-4\eta})$ and η being the threebody inelasticity parameter characterizing, for instance, the Efimov states lifetime and other universal properties of Efimov physics [48, 59]. [For 85 Rb, $E_c \approx 200$ kHz×h (or $10\mu K/k_B$) and displayed in Fig. 3 as a vertical dashed line. Figure 3(d) shows this change in behavior in our numerical calculations for $L_3(E)$ (solid line) along with the results for $L_3(E_q)$ obtained from the LL relation (1) (symbols), using our calculated values of E_q and Γ_q shown Fig. 3(a). As can be seen in Fig. 3(d), for ⁸⁵Rb, most of the states are in the $E_q > E_c$ regime where $L_3 = C_{\eta}/E_q^2$, in which case the LL relation (9) predicts $\Gamma_q = \Gamma_{\rm u}[1 - (\hbar\omega_{\rm ho})^2/E_q^2] \simeq \Gamma_{\rm u}[1 - 1/(2q + 3)^2],$ thus consistent with Γ_q being weakly dependent on E_q for states beyond $E_q = E_c$ [see Fig. 3(b)]. The unitary width, $\Gamma_{\rm u} = \hbar \omega_{\rm ho} (1 - e^{-4\eta})/\pi$, provides a direct mean

of extracting η from trap systems. In contrast, for ⁸⁷Rb atoms, the interaction is weak $(a = 1.21 \, r_{\rm vdW})$ and $L_3(E)$ is expected to be constant within a broader energy range $[E_c \approx 4000 \, {\rm kHz} \times h$ (or $200 \, \mu {\rm K}/k_B)$ for ⁸⁷Rb]. However, for ⁸⁷Rb, $L_3(E)$ is enhanced within this region due to the presence of a d-wave diatomic shape resonance [67], as shown by our numerical calculations for L_3 (solid line) in Fig. 3(c). Therefore, according to the LL relation (9), the primary mechanism responsible for the enhancement of Γ_q for ⁸⁷Rb trapped states in Fig. 3(a) traces back to the presence of the d-wave diatomic resonance. We note that the deviations shown in Fig. 3(c) near the position of the d-wave resonance are likely due to the couplings from other $\lambda \neq 0$ three-body channels, not included in our derivation of the LL relation.

We note that typical experiments with trapped fewatom systems require loading atoms from an ultracold gas into a single trap state. Without a dedicated cooling scheme (see, for instance, Refs. [20, 22, 45–47]), atoms will instead be loaded into the trap at some finite temperature, typically $k_BT \gg \hbar\omega_{\rm ho}$. In such cases, if the system is in thermal equilibrium, the LL relation can be extended by averaging Eq. (9) under a thermal distribution of quantum trapped states (see End Matter).

The LL relation (9) can be generalized to N-atom systems $(N \ge 2)$, in which case we obtained

$$\Gamma_{N,q} = \frac{1}{C_N} \frac{m^{\frac{3N-3}{2}}}{\hbar^{3N-5}} L_N(E_{N,q})
\times E_{N,q}^{\frac{3N-9}{2}} [E_{N,q}^2 - 4\alpha_N (\hbar\omega_{\text{ho}})^2] \omega_{\text{ho}},$$
(10)

with $C_N=\pi^{\frac{3N-3}{2}}N^{\frac{5}{2}}2^{\frac{3N-5}{2}}\Gamma[\frac{3N-3}{2}]$ and $\alpha_N=(N-1)(3N-7)(3N-5)/64$ (see details in Ref. [58] and further numerical tests at N=2). Here, $\Gamma_{N,q}$ and $E_{N,q}$ are the width and energy of the trapped N-body state, respectively, and L_N the free-space N-body loss coefficient [57, 68] for the J=0 and $\lambda=0$ partial-wave. For N>3, the width of an N-body trap state is typically determined by different decay pathways that may involve all or only some of the atoms. In Ref. [22], for instance, it was found experimentally that for Sr atoms in a q=0 state the decay rate for N=3, 4, and 5 is approximately proportional to the number of triads, indicating that three-body processes remain the dominant decay pathway. In reality, the direct experimental observable is the total decay rate, including all higher order processes, defined as,

$$\frac{\Gamma_{N,q}^{\text{tot}}}{h} = \sum_{K=3}^{N} {N \choose K} \frac{\Gamma_{K,q}}{h}$$

$$= {N \choose 3} \frac{\Gamma_{3,q}}{h} + {N \choose 4} \frac{\Gamma_{4,q}}{h} + \dots + \frac{\Gamma_{N,q}}{h}, \qquad (11)$$

with fundamental few-body decay rates $\Gamma_{K,q}/\hbar$ given in Eq. (10). In an experiment such as Ref. [22], where trap states containing $N = 3, 4, 5, \ldots$ atoms are prepared and

their decay rates $\Gamma_{N,q}^{\text{tot}}/\hbar$ measured, the corresponding fundamental rates can be extracted by inverting Eq. (11),

$$\frac{\Gamma_{N,q}}{\hbar} = \sum_{K=3}^{N} (-1)^{N-K} {N \choose K} \frac{\Gamma_{K,q}^{\text{tot}}}{\hbar}, \tag{12}$$

allowing for the determination of N-body scattering rates L_N via the LL relation (10), in a much more controlled way than in ultracold gas experiments [41–44, 68].

In summary, we have derived the Lellouch-Lüscher (LL) relation connecting the energy and width of fewbody states in a harmonic trap to the corresponding loss constants in free space, and demonstrated its validity through three-body numerical calculations. A unique feature of the LL relation is that, when atoms are prepared in trap states of a single partial wave—typically J = 0 for bosons—it enables the measurement of individual partial-wave contributions to loss rates. This makes trapped few-body systems a more sensitive probe of scattering resonances and interference phenomena, including those associated with Efimov physics [59, 69], which are often obscured in bulk-gas measurements due to thermal averaging over multiple partial waves [48]. We further show that the generalized N-body LL relation provides a systematic path to precise determinations of multi-body scattering rates [22, 57]. Taken together, the results from the LL relation framework help to establish trapped fewbody systems as a powerful platform for advancing our understanding of complex quantum phenomena.

This work was supported by the Baden-Württemberg Stiftung through the Internationale Spitzenforschung program (BWST, contract No. ISF2017-061) and by the German Research Foundation (DFG, Deutsche Forschungsgemeinschaft, contract No. 399903135). We acknowledge support from bwForCluster JUSTUS 2 for high performance computing. J.H.D and J.P.D. acknowledge funding by Q-DYNAMO (EU HORIZON-MSCA-2022- SE-01) within project No. 101131418. J.P.D. also acknowledges partial support from the U.S. National Science Foundation (PHY-2308791/PHYS-2452751) and the Office of Naval Research (ONR) grant N00014-21-1-2594.

End Matter

LL relation in thermal equilibrium

In experiments, loading a few atoms from the bulk into an isolated trap generally leads to $k_B T \gg \hbar \omega_{\rm ho}$, producing a thermal ensemble instead of a single trap state. The corresponding lifetime $h/\Gamma_{\rm th}$ of the thermal state can be estimated assuming a Boltzmann distribution of energies E_q as

$$\Gamma_{\rm th}(T) \equiv \frac{\sum_q e^{-E_q/k_B T} \Gamma_q}{\sum_q e^{-E_q/k_B T}}.$$
 (13)

Provided that the initial state (prior to loading) has a low enough temperature $(k_BT_{\rm in}\ll E_c)$ the populated trap states will predominantly be that of the J=0 (and $\lambda=0$) partial-wave. This allows us to use the LL relations [Eq. (9) or (10)] to derive simple results in two limiting cases, namely, the threshold $(|k_{\rm th}a|\ll 1)$ and unitary $(|k_{\rm th}a|\gg 1)$ regimes, with $\hbar k_{\rm th}=(mk_BT)^{1/2}$. In fact, while in the threshold regime most of the states that contribute to Eq. (13) are those with $\hbar \omega_{\rm ho}\ll E_q\sim k_BT\ll E_c$, where $L_3(E_q)\approx L_3(0)$, the states contributing to Eq. (13) in the unitary regime will be those with $\hbar \omega_{\rm ho}\ll E_c\ll E_q\sim k_BT$, where $L_3(E_q)=C_\eta/E_q^2$. Assuming $E_q\simeq (2q+3)\hbar \omega_{\rm ho}$ and using the LL relation (9), the thermal loss rate in Eq. (13) can be expressed as

$$\Gamma_{\rm th} = \begin{cases} 2\frac{1}{C} \frac{m^3}{h^4} L_3(0) (k_B T)^2 \omega_{\rm ho}, & \text{for } |k_{\rm th} a| \ll 1, \\ (1 - e^{-4\eta}) \hbar \omega_{\rm ho} / \pi = \Gamma_{\rm u}, & \text{for } |k_{\rm th} a| \gg 1, \end{cases}$$
(14)

for which a brief derivation and numerical test will be presented below. We note that for $|k_{\rm th}a| \ll 1$ the thermal decay rate is quadratic in (k_BT) and is a factor 2 larger than the rate obtained by LL relation (9), for $E_q = k_BT$ and $L_3(E_q) \simeq L_3(0)$. For $|k_{\rm th}a| \gg 1$, however, the thermal decay rate is independent on the temperature. This unexpected result is a direct consequence of the LL relation (9). Similar results can be obtained for N atoms in thermal equilibrium using the total decay rate in Eq. (11) and the corresponding LL relations (10).

To derive Eq. (14), we define the individual contribution of the qth trapped state to $\Gamma_{\rm th}$ as

$$\gamma_q = \frac{e^{-E_q/k_B T} \Gamma_q}{\sum_q e^{-E_q/k_B T}},\tag{15}$$

such that $\Gamma_{\rm th} = \sum_q \gamma_q$. Due to the Boltzmann factor e^{-E_q/k_BT} , temperature acts as a natural cutoff: a state will contribute significantly to $\Gamma_{\rm th}$ only if its energy E_q is of the order of $\sim k_BT$ or smaller. Consequently, in the threshold regime where $k_BT \ll E_c = \hbar^2/ma^2$, the major contributing states have energies $\hbar\omega_{\rm ho} \ll E_q \ll E_c$. This is demonstrated in Fig. 4(a) by using the following toy

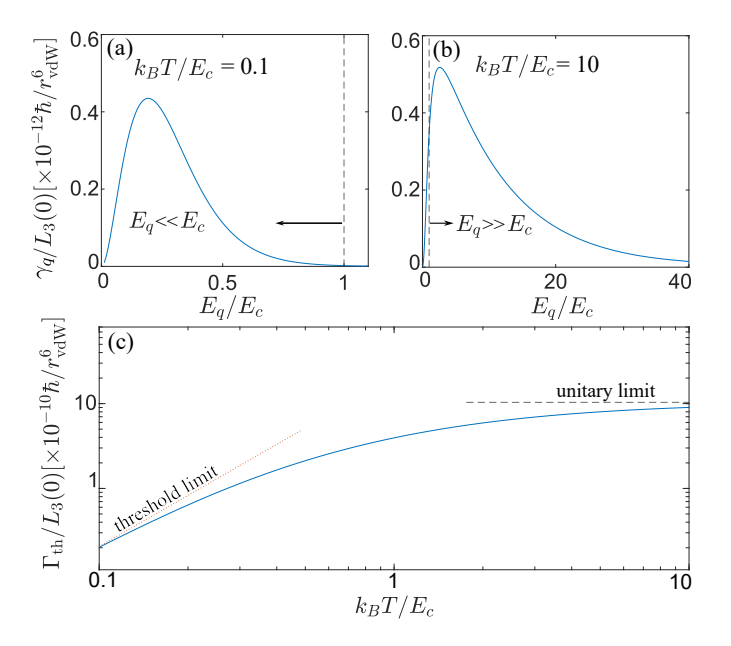


FIG. 4. The distribution of the individual contribution, γ_q , of the trap state to $\Gamma_{\rm th}$ in the threshold regime of $k_BT/E_c=0.1$ (a) and in the unitary regime of $k_BT/E_c=10$ (b). The vertical dashed lines indicate that $E_q=E_c$. (c) shows the temperature dependence behavior of $\Gamma_{\rm th}$ calculated from Eq. (13) and from Eq. (14) at threshold limit (dotted line) and unitary limit (dashed line). The displayed result is obtained by using Eq. (16) for $L_3(E)$ with $\alpha=1$, $E_c=0.1E_{\rm vdW}$ and $\hbar\omega_{\rm ho}=0.001E_{\rm vdW}$ and Eq. (9) for Γ_q , for instance.

model for $L_3(E)$

$$L_3(E) = \frac{L_3(0)}{1 + \alpha (E/E_c)^2},\tag{16}$$

where $\alpha = L_3(0)E_c^2/C_\eta$. [This toy model is designed to capture the two limiting behaviors of $L_3(E)$: $L_3(E) \rightarrow L_3(0)$ as $E \rightarrow 0$ (threshold limit) and $L_3(E) \rightarrow C\eta/E^2$ as $E \rightarrow \infty$ (unitary limit), thus providing a suitable framework for the analysis in this section.]

As the majority contribution to $\Gamma_{\rm th}$ comes from the states with $\hbar\omega_{\rm ho}\ll E_q\ll E_c$, we are allowed to replace the energy dependence $L_3(E)$ with $L_3(0)$ and $[E_q^2-\hbar^2\omega_{\rm ho}^2]$ with E_q^2 in Eq. (13). By further assuming $E_q\simeq (2q+3)\hbar\omega_{\rm ho}$, we get

$$\Gamma_{\rm th} = \frac{1}{C} \frac{m^3}{\hbar^2} L_3(0) \omega_{\rm ho}^3 g\left(\frac{\hbar \omega_{\rm ho}}{k_b T}\right),\tag{17}$$

with

$$g(x) = 5 + 4 \coth(x) + 2 \operatorname{csch}^{2}(x)$$

$$= \frac{2}{x^{2}} + \frac{4}{x} + \frac{13}{3} + O(x),$$
(18)

where the leading order gives Eq. (14) at $|k_{\rm th}a| \ll 1$. The validity of our Eq. (14) is demonstrated in Fig. 4(c),

where it is compared to the numerical result using the expression (16) for $L_3(E)$.

At the unitary limit where $k_BT\gg E_c$, the states that contribute to $\Gamma_{\rm th}$ still have a E_q of the order of $\sim k_BT$ or smaller. However, in this regime, a majority of these states can satisfy $E_q\gg E_c\gg \hbar\omega_{\rm ho}$ (see Fig. 4(b)), such that $L_3(E_q)=C_\eta/E_q^2$. To further simplify the derivation, we assume $C_\eta=L_3(E_q)E_q^2$ for all states. Plugging this expression into Eq. (13) and by considering $[E_q^2-\hbar^2\omega_{\rm ho}^2]\to E_q^2$, we get the simple relation in Eq. (14), i.e., $\Gamma_{\rm th}=\Gamma_{\rm u}$. The validity of Eq. (14) in this limit is also confirmed in Fig. 4(c) by comparing it to the numerical result from the toy model.

Supplemental Material

Hyperspherical Adiabatic Representation

In the hyperspherical adiabatic representation, the total wave function $\Psi(R,\Omega)$ of three atoms can be expressed as [54, 55]:

$$\Psi(R,\Omega) = \sum_{\nu} F_{\nu}(R)\Phi_{\nu}(R;\Omega), \tag{19}$$

where $F_{\nu}(R)$ is determined by the hyperradial equation (2) in the main text and $\Phi_{\nu}(R;\Omega)$ are the eigenfunctions of the adiabatic hyperangular equation:

$$\hat{H}_{\rm ad}\Phi_{\nu}(R;\Omega) = U_{\nu}(R)\Phi_{\nu}(R;\Omega) \tag{20}$$

at fixed R. Here Ω denotes a set of hyperangles describing the internal motion of the three-atom system.

To solve the adiabatic hyperangular equation (20), we use the same interaction model as in Ref. [56], which we briefly introduce below. The adiabatic Hamiltonian \hat{H}_{ad} ,

$$\hat{H}_{\rm ad} = \frac{\hat{\Lambda}^2(\Omega) + 15/4}{2\mu R^2} \hbar^2 + \hat{V}_T(R, \Omega) + \hat{H}_{\rm hf+Z}(B), \quad (21)$$

contains the hyperangular kinetic energy via the hyperangular momentum operator [54, 55], $\hat{\Lambda}$, the hyperfine and Zeeman Hamiltonian, H_{hf+Z} , as well as all the interatomic interactions, $V_T(R,\Omega) = V(r_{12}) + V(r_{23}) + V(r_{31})$. We note that the Zeeman interaction disappears in the present study as we consider B = 0. The pairwise interatomic interaction, $\hat{V}(r_{ij}) = \sum_{SM_S} |SM_S\rangle V_S(r_{ij})\langle SM_S|,$ is represented by realistic singlet (S = 0) and triplet (S = 1) Bohr-Oppenheimer potentials, where S is the total electronic spin and M_S is azimuthal projection. At long range, both singlet and triplet potentials are dominated by the van der Waals interaction, characterized by the length $r_{\rm vdW}=(mC_6/\hbar^2)^{1/4}/2$ and energy $E_{\rm vdW}=\hbar^2/mr_{\rm vdW}^2$ scales, where C_6 is the van der Waals dispersion coefficient [10]. In this work, we focus on ⁸⁵Rb₂ and ⁸⁷Rb₂, for which the characteristic length scale are $r_{\text{vdW}} \approx 82.16a_0$ and $r_{\text{vdW}} \approx 82.64a_0$, respectively [66]. Here, a_0 denotes the Bohr radius. To reduce the computational burden, we add a short-range repulsive term for each potential to control the number of bound states in the system [66]. As a result, each interaction potential has 6 s-wave bound states except that the triplet potential of 85 Rb₂ has 5 s-wave bound states. Nevertheless, the reduced singlet and triplet potentials successfully reproduce the weakly bound states and the low-energy scattering properties.

The solutions of the hyperangular adiabatic equation are obtained by expanding the channel functions Φ_{ν} on the basis of separated atoms hyperfine spins states, $|\sigma\rangle \equiv |f_i m_{f_i}\rangle |f_j m_{f_j}\rangle |f_k, m_{f_k}\rangle$,

$$\Phi_{\nu}(R;\Omega) = \sum_{\sigma} \phi_{\nu}^{\sigma}(R;\Omega) |\sigma\rangle, \tag{22}$$

where f and m_f denote the atomic hyperfine and its magnetic projection quantum numbers, respectively. In practice, we fix the third (k) atom's spin at its initial state, i.e., $|f_k, m_{f_k}\rangle = |f_k^{\rm in}, m_{f_k}^{\rm in}\rangle$. We note that the validity of fixing the third atom's spin has been for Rb in Ref. [56]. In this work, the initial atomic spin state is chosen as $|f_k^{\rm in}, m_{f_k}^{\rm in}\rangle = |2, -2\rangle$ for ⁸⁵Rb and $|1, -1\rangle$ for ⁸⁷Rb, respectively. Applying this expansion to the hyperangular adiabatic equation results in a coupled system of equations for the components of $\phi_{\nu}^{\rm in}$:

$$\left[\frac{\hat{\Lambda}^{2}(\Omega) + 15/4}{2\mu R^{2}}\hbar^{2} + E_{\rm hf}^{\sigma}(B) - U_{\nu}(R)\right]\phi_{\nu}^{\sigma}(R;\Omega)
+ \sum_{\sigma'} V_{T}^{\sigma\sigma'}(R,\Omega)\phi_{\nu}^{\sigma'}(R;\Omega) = 0, \quad (23)$$

where $E_{\rm hf}^{\sigma}$ is the sum of the hyperfine energies of the three separated atoms in the $|\sigma\rangle$ spin state at the magnetic field B. After Eq. (23), the adiabatic potentials W_{ν} and non-adiabatic couplings $W_{\nu\nu'}$ can be obtained for the use in hyperradial equation (2) [54, 55]. The adiabatic potentials have two possible asymptotic $(R \to \infty)$ forms:

$$W_{\nu}(R) = W_f(R) \simeq -E_b + \frac{l(l+1)}{2uR^2}\hbar^2,$$
 (24)

$$W_{\nu}(R) = W_{\lambda}^{b}(R) \simeq E_{\rm hf}^{\sigma} + \frac{\lambda(\lambda+4) + 15/4}{2\mu R^{2}} h^{2},$$
 (25)

defining the atom-molecule decay channels (labelled by f) and three-atom continuum channels (labelled by λ), respectively. Here, E_b denotes the molecular binding energy. In the present work, the total number of atom-molecule decay channels is 112 for both $^{85}{\rm Rb}$ and $^{87}{\rm Rb}$, including molecular states with all possible spins and partial waves. The continuum three-body channels are included up to several tens to ensure good convergence.

In our calculations for three atoms in an isotropic harmonic trap $(\omega_x = \omega_y = \omega_z = \omega_{ho})$, adding the trap in our model only affects the hyperradial motion, leaving the hyperangular motion unchanged. Therefore, the effect of the isotropic harmonic trap is captured by adding $\frac{1}{2}\mu\omega_{\rm ho}^2R^2$ to free-space equation (2). For numerical implementation, it is both practical and physically reasonable to include the trap potential only in the three-atom continuum channels W_{λ} , while leaving all atom-dimer channels W_f unconfined to allow decays [22, 29]. This choice is motivated by the fact that the trap depth is typically much smaller than the kinetic energy released during molecule formation via decay pathways. As a result, the influence of the trap on the recombination dynamics within W_f channels is negligible. The trapped state is then obtained from a standard atom-dimer scattering calculation in the relevant energy regime, where the resonance feature is identified.

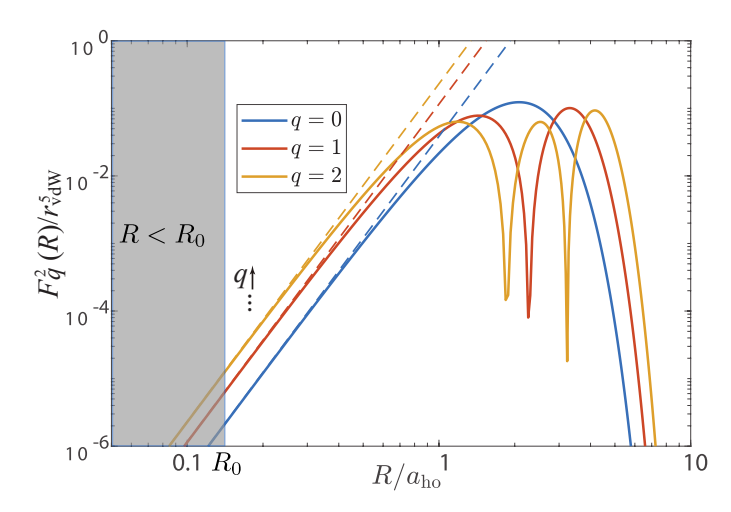


FIG. 5. Non-interacting three-body hyperradial wavefunction $F_q(R)$ in a spherical harmonic trap. The solid lines show $F_q^2(R)$ from Eq. (7), while the dashed lines represent the corresponding Taylor expansion to the leading order. The shaded area indicates the reaction regime $R < R_0$.

Mean inelastic three-body probability density \mathcal{D}_q

We define the reactive three-body probability density \mathcal{D}_q :

$$\mathcal{D}_{q} \equiv \frac{1}{\mathcal{V}_{0}} \iint_{\mathcal{V}_{0}} |\Psi_{3,q}(\vec{R}_{cm}, \vec{R})|^{2} d^{3} \vec{R}_{cm} d^{3} \vec{R}, \quad (26)$$

by averaging the probability density of the wavefunction $\Psi_{3,q}(\vec{R}_{\rm cm},\vec{R})$ for q-th trapped three-body state over the hyperspherical volume $V_0 = \pi^3 R_0^6/6$ within the reaction regime ($|\vec{R}| < R_0$). The parameter R_0 , characterizing the recombination regime, is expected to be of the order of the interaction range. For van der Waals interaction, for instance, we consider $R_0 \sim r_{\text{vdW}} = \frac{1}{2} (mC_6 \hbar^2)^{1/4}$, where C_6 is the dispersion coefficient. Here, $\Psi_{3,q}(\vec{R}_{\rm cm},\vec{R})$ describes both the 3D center of mass motion in \vec{R}_{cm} and 6D relative motion in $R = (R, \Omega)$. We note that the center of mass motion is not essential for defining \mathcal{D}_q as it does not play a role in the reaction process. Nevertheless, we keep it in our definition (26) for completeness. In the hyperspherical coordinate representation, we consider only the incoming $\lambda = 0$ channel to express the trapped three-body wavefunction as $\Psi_{3,q}(\vec{R}_{cm},\vec{R}) = \Psi_{cm}(\vec{R}_{cm})\Phi_0(R;\Omega)F_q(R)R^{-5/2}$, normalized by $\int |\Psi_{\rm cm}(\vec{R}_{\rm cm})|^2 d^3\vec{R}_{\rm cm} = 1$, $\int |\Phi_0(R;\Omega)|^2 d\Omega = 1$ and $\int |F_q(R)|^2 dR = 1$. By using $d^3\vec{R} = R^5 dR d\Omega$ and integrating over $\vec{R}_{\rm cm}$ and Ω in Eq. (26), we get

$$\mathcal{D}_{q} = \frac{1}{\mathcal{V}_{0}} \int_{0}^{R_{0}} F_{q}(R)^{2} dR. \tag{27}$$

We then apply the Taylor expansion around (R = 0) to the non-interacting three-body trap-state wavefunction $F_q^2(R)$ [given by Eq. (7)]:

$$F_q^2(R) = \frac{R^5}{N_q a_{\text{ho}}^6} \left[\left(\frac{\Gamma(q+3)}{q!\Gamma(3)} \right)^2 + O\left(\frac{R^2}{\sqrt{3}a_{\text{ho}}^2} \right) \right].$$
 (28)

We neglect the $O\left(\frac{R^2}{\sqrt{3}a_{\text{ho}}^2}\right)$ terms, which is justified by the assumption $R_0 \sim r_{\text{vdW}} \ll a_{\text{ho}}$ (see, for example, Fig. 5). As a result, we get to the leading order

$$\mathcal{D}_{q} = \frac{12 \int_{0}^{R_{0}} R^{5} dR}{\pi^{3} R_{0}^{6} (q+1) (q+2) 3 \sqrt{3} a_{\text{ho}}^{6}} \left(\frac{\Gamma(q+3)}{q! \Gamma(3)} \right)^{2}$$
(29)
$$= \frac{(q+1) (q+2)}{6 \sqrt{3} \pi^{3} a_{\text{ho}}^{6}} = \frac{m^{3} \omega_{\text{ho}} (E_{q}^{2} - h^{2} \omega_{\text{ho}}^{2})}{24 \sqrt{3} \pi^{3} h^{5}},$$

where we make the substitution $(2q+3)\hbar\omega_{\text{ho}} \to E_q$. This allows us to use the actual trapped-state energy E_q for \mathcal{D}_q , thereby capturing (at least partially) the modification due to interactions.

According to Eq. (29), the reactive three-body probability density increases with the trap frequency ω_{ho} as a higher ω_{ho} typically compresses the occupied volume and raises the particle density. For a given $a_{\rm ho}$, however, the reactive three-body probability density \mathcal{D}_q increases with the energy of the trap state E_q (or equivalently with the state index q), even though the state size expands as $(2q+3)^{1/2}a_{\text{ho}}$. This behavior arises because the wavefunction amplitude at short range $(R \ll a_{\text{ho}})$ increases with the trap state index q, as is shown in Fig. 5. At the same time, Fig. 5 also shows that the wavefunction amplitude grows at long-range $(R \gg a_{\rm ho})$ with an increasing q, leading to an overall increase in the state size. That is to say, as q increases, the wavefunction amplitude in the trap state is pushed toward both short- and long-range regions, resulting in a higher reactive probability density \mathcal{V}_0 as the trap state expands. Note that the short-range parameter R_0 does not appear in Eq. (29) because it cancels between the integration contribution and \mathcal{V}_0 in Eq. (38). Consequently, the precise choice of R_0 will not affect the physical result. Practically, $R_0 = \beta r_{\rm vdW}$ can be chosen to scale with the characteristic length scale, $r_{\rm vdW}$, of the van der Waals interaction between atoms. A reasonable value for β is considered to be $1 \leq \beta \ll \frac{a_{\text{ho}}}{r_{\text{vdW}}}.$

Connection \mathcal{D}_q to the three-body correlation function

For our purpose of this subsection, we rewrite Eq. (26) as:

$$\mathcal{D}_q = \frac{1}{\pi^3} \iint I_{R_0}(\vec{R}_{cm}, \Omega) d^3 \vec{R}_{cm} d\Omega$$
 (30)

with

$$I_{R_0}(\vec{R}_{cm}, \Omega) = \frac{6}{R_0^6} \int_0^{R_0} |\Psi_{3,q}(\vec{R}_{cm}, \vec{R})|^2 R^5 dR.$$
 (31)

Building on the fact that the three-body correlation function is defined in the context of contact interactions [33], we take the limit $R_0 \to 0$, yielding

$$I_{R_0 \to 0}(\vec{R}_{cm}, \Omega) = |\Psi_{3,q}(\vec{R}_{cm}, \vec{R})|_{R=0}^2$$
$$= \int |\Psi_{3,q}(\vec{R}_{cm}, \vec{R})|^2 \delta(R) dR. \quad (32)$$

By plugging the above expression of $I_{R_0\to 0}(\vec{R}_{\rm cm},\Omega)$ into Eq. (30), we get

$$\lim_{R_{0}\to 0} \mathcal{D}_{q} = \frac{1}{\pi^{3}} \iiint |\Psi_{3,q}(\vec{R}_{cm}, \vec{R})|^{2} \delta(R) d^{3} \vec{R}_{cm} dR d\Omega$$

$$= \iiint |\Psi_{3,q}(\vec{R}_{cm}, \vec{R})|^{2} \delta(\vec{R}) d^{3} \vec{R}_{cm} d^{3} \vec{R}$$

$$= \iiint |\Psi_{3,q}(\vec{R}_{cm}, \vec{R})|^{2} \delta(\vec{\rho}_{23}) \delta(\vec{\rho}_{1}) d^{3} \vec{R}_{cm} d^{3} \vec{\rho}_{23} d^{3} \vec{\rho}_{1}$$
(33)

where we use $\delta(\vec{R}) = \delta(R)/(\pi^3 R^5)$ and $d\vec{R} = R^5 dR d\Omega$ to get the second line. The 6D position vector $\vec{R} = (R, \Omega)$ in relative motion can also be decomposed in Jacobi coordinates $\vec{R} = (s_k^{-1} \vec{\rho}_{ij}, s_k \vec{\rho}_k)$ with $i \neq j \neq k$, where $\vec{\rho}_{ij} = \vec{r}_i - \vec{r}_j$, $\vec{\rho}_k = \vec{r}_k - (\vec{r}_i + \vec{r}_j)/2$, $s_i = s_j = s_k = s = 2^{1/2}/3^{1/4}$ for identical particles [59]. From the second to the third line of the above equation, we take $\vec{R} = (s^{-1} \vec{\rho}_{23}, s \vec{\rho}_1)$, for instance, which results in $\delta(\vec{R}) = \delta(s^{-1} \vec{\rho}_{23})\delta(s\vec{\rho}_1) = \delta(\vec{\rho}_{23})\delta(\vec{\rho}_1)$ and $d\vec{R} = d(s^{-1} \vec{\rho}_{23})d(s\vec{\rho}_1) = d\vec{\rho}_{23}d\vec{\rho}_1$. Here $\vec{r}_1, \vec{r}_2, \vec{r}_3$ denote the single-atom 3D position vectors, where \vec{R}_{cm} is given by $\vec{R}_{cm} = (\vec{r}_1 + \vec{r}_2 + \vec{r}_3)/3$. Next, we take q = 0 and make the following transformation on the three-body total wavefunction

$$\begin{split} &\Psi_{3,q=0}[\vec{R}_{\rm cm}, \vec{R} \to (s^{-1}\vec{\rho}_{23}, s\vec{\rho}_{1})] = \langle \vec{R}_{\rm cm}, \vec{\rho}_{23}, \vec{\rho}_{1} | \Psi_{3,0} \rangle \\ &= \iiint \langle \vec{R}_{\rm cm}, \vec{\rho}_{23}, \vec{\rho}_{1} | \vec{r}_{1}, \vec{r}_{2}, \vec{r}_{3} \rangle \langle \vec{r}_{1}, \vec{r}_{2}, \vec{r}_{3} | \Psi_{3,0} \rangle d^{3}\vec{r}_{1} d^{3}\vec{r}_{2} d^{3}\vec{r}_{3} \\ &= \iiint \delta \left(\vec{R}_{\rm cm} - \frac{\vec{r}_{1} + \vec{r}_{2} + \vec{r}_{3}}{3} \right) \delta(\vec{\rho}_{23} - \vec{r}_{2} + \vec{r}_{3}) \\ &\times \delta(\vec{\rho}_{1} - \vec{r}_{1} + \frac{\vec{r}_{2} + \vec{r}_{3}}{2}) \phi_{0}(\vec{r}_{1}) \phi_{0}(\vec{r}_{2}) \phi_{0}(\vec{r}_{3}) d^{3}\vec{r}_{1} d^{3}\vec{r}_{2} d^{3}\vec{r}_{3}, \end{split}$$

$$(34)$$

where ϕ_0 denotes the single-particle ground-state wavefunction of the trap. By substituting Eq. (34) into Eq. (33) and integrating over $\vec{R}_{\rm cm}$, $\vec{\rho}_{23}$ and $\vec{\rho}_1$, we obtain

$$\lim_{R_0 \to 0} \mathcal{D}_0 = \iiint |\phi_0(\vec{r}_1)\phi_0(\vec{r}_2)\phi_0(\vec{r}_3)|^2$$

$$\times \delta(\vec{r}_2 - \vec{r}_3)\delta(\vec{r}_3 - \vec{r}_1)d^3\vec{r}_1d^3\vec{r}_2d^3\vec{r}_3$$

$$= \int |\phi_0(\vec{r})|^6d^3\vec{r}.$$
(35)

As a result, our LL relation (9), when applied to the ground trapped state, reduces to the commonly used near-threshold relation: $\Gamma/\hbar = L_3 \int d\vec{r} |\phi_0(r)|^6/3$ [22, 33, 70, 71].

We observe that the right-hand side of Eq. (35) can be identified as the three-body correlation function for three particles [33]. Accordingly, the reactive three-body probability density \mathcal{D}_q defined in the present work can be interpreted as a generalized three-body correlation function for the qth trapped three-body state. Equation (29), as discussed previously, predicts a linear dependence of the generalized three-body correlation function on the trap frequency ω_{ho} and a quadratic dependence on the trapped-state energy E_q .

Time-delay discussion

We fit the time delay τ_D to the following Lorentzian form

$$\tau_D(E) = \frac{\hbar \Gamma_q}{(E - E_q)^2 + (\Gamma_q/2)^2} + \tau_{\text{Dbg}}, \tag{36}$$

where an additional parameter τ_{Dbg} is included to describe the local background time delay. The background parameter τ_{Dbg} improves fit performance. We note that with τ_{Dbg} the width of trapped state is given by $\Gamma_q = 4\hbar/[\tau_D(E_q) - \tau_{\mathrm{Dbg}}]$, slightly modified from the relation, $\Gamma_q = 4\hbar/\tau_D(E_q)$, given by a standard Lorentzian. The background time delay can also provide valuable physical insights into the system. For instance, the sign of its value at the threshold is negative and positive for the ⁸⁵Rb and ⁸⁷Rb, respectively. This reflects correctly the attractive interaction (a < 0) between ⁸⁵Rb atoms and the repulsive (a > 0) interaction between ⁸⁷Rb atoms at low energies. Nevertheless, further discussions on τ_{Dbg} are beyond the scope of the present work.

Lellouch-Lüscher relation for N-body losses

In this section, we generalize the LL relation (9) to connect the free-space N-body loss rate coefficient $L_N(E_{N,q})$ [57, 68] with the energy $E_{N,q}$ and width $\Gamma_{N,q}$ of a trapped N-body state, and the trap frequency ω_{ho} . We initially consider N-body loss (i.e. each loss event involving N particles) as the dominant decay pathway of an N-body state, but will later show that this limitation is not essential. Consequently, we have

$$\frac{\Gamma_{N,q}}{\hbar} = \frac{L_N(E_{N,q})}{N} \mathcal{D}_{N,q},\tag{37}$$

where the N-body reactive probability density $\mathcal{D}_{N,q}$ is given by

$$\mathcal{D}_{N,q} = \frac{1}{\mathcal{V}_{N,0}} \int_0^{R_{N,0}} F_{N,q}(R_N)^2 dR_N, \tag{38}$$

within the hyperspherical volume $\mathcal{V}_{N,0} = \frac{\pi^{\frac{3N-3}{2}}R_{N,0}^{3N-3}/\Gamma(\frac{3N-1}{2})}{(R_N < R_{N,0})}$. Here, R_N is the N-body hyperradius describing the overall size and $\Gamma(\cdot)$ denotes the Gamma

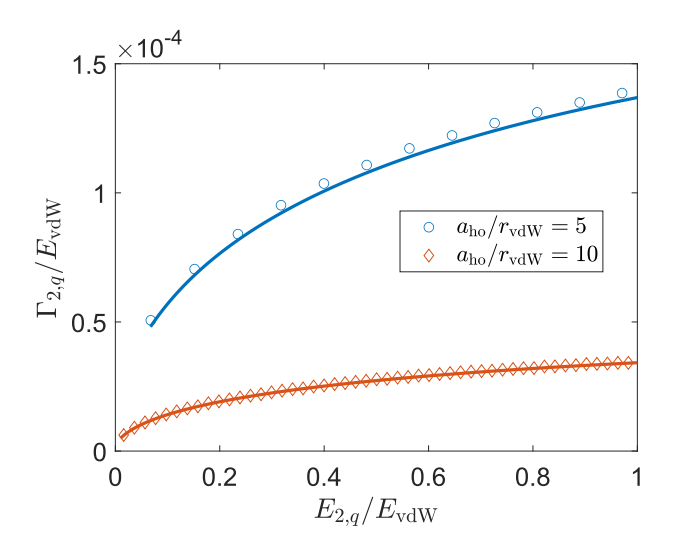


FIG. 6. The width $\Gamma_{2,q}$ of trapped two-body state versus its energy $E_{2,q}$ for ⁸⁷Rb in $|2,-1\rangle$ state at B=1000 G. The data symbols represent results obtained by fitting the two-body time delay at $a_{\rm ho}/r_{\rm vdW}=5$ (circles) and 10 (diamonds) to a Lorentzian form, while the solid line corresponds to the prediction from Eq. (45).

function. The non-interacting N-body wavefunction reads

$$F_{N,q}(R_N) = \frac{1}{\sqrt{M_{N,q}}} R_N^{\frac{3N-4}{2}} e^{\left[-R_N^2/(2N^{\frac{1}{N-1}} a_{\text{ho}}^2)\right]}$$
(39)

$$\times L_q^{\left(\frac{3N-5}{2}\right)} \left[R_N^2/(N^{\frac{1}{N-1}} a_{\text{ho}}^2)\right],$$

with a normalization factor $M_{N,q}$ given by

$$M_{N,q} = \frac{N^{3/2}\Gamma(q + \frac{3N-3}{2})}{2\Gamma(q+1)} a_{\text{ho}}^{3N-3}.$$
 (40)

Similar to the previous derivation in the three-body case, we assume $R_{N,0} \ll a_{\text{ho}}$ and retain only the leading-order contribution:

$$\mathcal{D}_{N,q} = \frac{1}{M_{N,q} \mathcal{V}_{N,0}} \left(\frac{\Gamma(q + \frac{3N-3}{2})}{q! \Gamma(\frac{3N-3}{2})} \right)^2 \int_0^{R_{N,0}} R_N^{3N-4} dR_N$$
$$= \frac{1}{a_{\text{ho}}^{3N-3} \pi^{\frac{3N-3}{2}} N^{3/2} \Gamma(\frac{3N-3}{2})} \frac{\Gamma(\frac{3N-3}{2} + q)}{\Gamma(1+q)}, \quad (41)$$

or, defining q from its relationship with $E_{N,q} = [2q + (3N - 3)/2]\hbar\omega_{\text{ho}}$,

$$\mathcal{D}_{N,q} = \frac{\Gamma(\frac{E_q}{2\hbar\omega_{\text{ho}}} + \frac{3N-3}{4})/\Gamma(\frac{E_q}{2\hbar\omega_{\text{ho}}} - \frac{3N-7}{4})}{a_{\text{ho}}^{3N-3}\pi^{\frac{3N-3}{2}}N^{3/2}\Gamma(\frac{3N-3}{2})},$$
 (42)

The above equation can be further simplifies by employing the asymptotic form of the function below for large x:

$$\frac{\Gamma(x + \frac{3N-3}{4})}{\Gamma(x - \frac{3N-7}{4})} = x^{\frac{3N-5}{2}} \left(1 - \frac{\alpha_N}{x^2} + \frac{\beta_N}{x^4} + \cdots \right) \tag{43}$$

where $\alpha_N = (N-1)(3N-7)(3N-5)/64$, and $\beta_N = (N-3)(N-1)(3N-11)(3N-7)(3N-5)(15N-11)/40960$. For simplicity, we truncate to the $1/x^2$ term and get

$$\mathcal{D}_{N,q} \simeq \frac{\left(\frac{E_q}{2\hbar\omega_{\text{ho}}}\right)^{\frac{3N-5}{2}} \left[1 - \alpha_N / \left(\frac{E_q}{2\hbar\omega_{\text{ho}}}\right)^2\right]}{a_{\text{ho}}^{3N-3} \pi^{\frac{3N-3}{2}} N^{3/2} \Gamma\left(\frac{3N-3}{2}\right)}$$

$$= \frac{\left(\frac{1}{2\hbar\omega_{\text{ho}}}\right)^{\frac{3N-5}{2}} E_q^{\frac{3N-9}{2}} \left[E_q^2 - 4\alpha_N (\hbar\omega_{\text{ho}})^2\right]}{a_{\text{ho}}^{3N-3} \pi^{\frac{3N-3}{2}} N^{3/2} \Gamma\left(\frac{3N-3}{2}\right)}.$$
 (44)

Note that for N=3 the above expression is exact because $\beta_3=0$ and all higher-order coefficients vanish. For other values of N, the asymptotic expression for \mathcal{D}_q above leads to a relative error below 10% for $E_{q=0}$ and $N \leq 5$, and decreases rapidly as $1/E_q^4$ for larger values of $E_{q>0}$ for all N. By substituting Eq. (44) into Eq. (37), we then get

$$\Gamma_{N,q} = \frac{1}{2^{\frac{3N-5}{2}} \pi^{\frac{3N-3}{2}} N^{\frac{5}{2}} \Gamma(\frac{3N-3}{2})} \frac{m^{\frac{3N-3}{2}}}{\hbar^{3N-5}} L_N(E_{N,q}) \times E_{N,q}^{\frac{3N-9}{2}} [E_q^2 - 4\alpha_N(\hbar\omega_{\text{ho}})^2] \omega_{\text{ho}}, \tag{45}$$

leading to the result expressed in Eq. (10) of the main text. In the case N=3, the above expression subsumes Eq. (9), with its validity convincingly validated in the main text. For N=2, we also demonstrate the validity of Eq. (45) by considering ⁸⁷Rb atoms in $|2,-1\rangle$ state and calculating free-space two-body loss rate as well as the width and energy of the trapped two-body state at B=1000 G, as is shown in Fig. 6. Here, the decay originates from the relaxation of atoms from higher to lower hyperfine states. A magnetic field of B=1000 G is chosen to guarantee that the released energy is sufficient for the atoms to leave the trap following decay.

- * Jinglun.Li@ist.ac.at
- † Jose.DIncao@umb.edu
- I. Bloch, Ultracold quantum gases in optical lattices, Nature Physics 1, 23 (2005).
- [2] I. Bloch and M. Greiner, Exploring Quantum Matter with Ultracold Atoms in Optical Lattices, edited by P. Berman and C. Lin, Advances In Atomic, Molecular, and Optical Physics, Vol. 52 (Academic Press, 2005) pp. 1–47.
- [3] F. Schäfer, T. Fukuhara, S. Sugawa, Y. Takasu, and Y. Takahashi, Tools for quantum simulation with ultracold atoms in optical lattices, Nature Reviews Physics 2, 411 (2020).
- [4] B. J. Lester, Y. Lin, M. O. Brown, A. M. Kaufman, R. J. Ball, E. Knill, A. M. Rey, and C. A. Regal, Measurement-based entanglement of noninteracting bosonic atoms, Phys. Rev. Lett. 120, 193602 (2018).
- [5] A. M. Kaufman, M. C. Tichy, F. Mintert, A. M. Rey, and C. A. Regal, Chapter Seven - The Hong-Ou-Mandel Effect With Atoms (Academic Press, 2018) pp. 377-427.
- [6] L. Anderegg, L. W. Cheuk, Y. Bao, S. Burchesky, W. Ketterle, K.-K. Ni, and J. M. Doyle, An optical

- tweezer array of ultracold molecules, Science **365**, 1156 (2019).
- [7] A. I. Krylov, J. Doyle, and K.-K. Ni, Quantum computing and quantum information storage, Phys. Chem. Chem. Phys. 23, 6341 (2021).
- [8] I. Bloch, J. Dalibard, and W. Zwerger, Many-body physics with ultracold gases, Rev. Mod. Phys. 80, 885 (2008).
- [9] M. Lewenstein, A. Sanpera, V. Ahufinger, B. Damski, A. Sen(De), and U. Sen, Ultracold atomic gases in optical lattices: mimicking condensed matter physics and beyond, Advances in Physics 56, 243 (2007).
- [10] C. Chin, R. Grimm, P. Julienne, and E. Tiesinga, Fesh-bach resonances in ultracold gases, Rev. Mod. Phys. 82, 1225 (2010).
- [11] A. M. Kaufman, B. J. Lester, and C. A. Regal, Cooling a single atom in an optical tweezer to its quantum ground state, Phys. Rev. X 2, 041014 (2012).
- [12] J. Fortágh and C. Zimmermann, Magnetic microtraps for ultracold atoms, Rev. Mod. Phys. 79, 235 (2007).
- [13] G. Gauthier, T. A. Bell, A. B. Stilgoe, M. Baker, H. Rubinsztein-Dunlop, and T. W. Neely, Chapter one - dynamic high-resolution optical trapping of ultracold atoms (Academic Press, 2021) pp. 1–101.
- [14] H. Ott, Single atom detection in ultracold quantum gases: a review of current progress, Reports on Progress in Physics 79, 054401 (2016).
- [15] A. M. Kaufman and K.-K. Ni, Quantum science with optical tweezer arrays of ultracold atoms and molecules, Nature Physics 17, 1324 (2021).
- [16] M. F. Andersen, Optical tweezers for a bottom-up assembly of few-atom systems, Advances in Physics: X 7, 2064231 (2022).
- [17] S. K. Pampel, M. Marinelli, M. O. Brown, J. P. D'Incao, and C. A. Regal, Quantifying light-assisted collisions in optical tweezers across the hyperfine spectrum (2024), arXiv:2408.15359.
- [18] M. O. Brown, T. Thiele, C. Kiehl, T.-W. Hsu, and C. A. Regal, Gray-molasses optical-tweezer loading: Controlling collisions for scaling atom-array assembly, Phys. Rev. X 9, 011057 (2019).
- [19] L. R. Liu, J. D. Hood, Y. Yu, J. T. Zhang, N. R. Hutzler, T. Rosenband, and K.-K. Ni, Building one molecule from a reservoir of two atoms, Science 360, 900 (2018).
- [20] L. R. Liu, J. D. Hood, Y. Yu, J. T. Zhang, K. Wang, Y.-W. Lin, T. Rosenband, and K.-K. Ni, Molecular assembly of ground-state cooled single atoms, Phys. Rev. X 9, 021039 (2019).
- [21] J. T. Zhang, Y. Yu, W. B. Cairncross, K. Wang, L. R. B. Picard, J. D. Hood, Y.-W. Lin, J. M. Hutson, and K.-K. Ni, Forming a single molecule by magnetoassociation in an optical tweezer, Phys. Rev. Lett. 124, 253401 (2020).
- [22] A. Goban, R. B. Hutson, G. E. Marti, S. L. Campbell, M. A. Perlin, P. S. Julienne, J. P. D'Incao, A. M. Rey, and J. Ye, Emergence of multi-body interactions in a fermionic lattice clock, Nature 563, 369 (2018).
- [23] A. N. Wenz, G. Zürn, S. Murmann, I. Brouzos, T. Lompe, and S. Jochim, From Few to Many: Observing the Formation of a Fermi Sea One Atom at a Time, Science 342, 457 (2013).
- [24] F. H. Mies, E. Tiesinga, and P. S. Julienne, Manipulation of feshbach resonances in ultracold atomic collisions using time-dependent magnetic fields, Phys. Rev. A 61, 022721 (2000).

- [25] M. Greiner, O. Mandel, T. W. Hänsch, and I. Bloch, Collapse and revival of the matter wave field of a Bose– Einstein condensate, Nature 419, 51 (2002).
- [26] C. Ospelkaus, S. Ospelkaus, L. Humbert, P. Ernst, K. Sengstock, and K. Bongs, Ultracold Heteronuclear Molecules in a 3D Optical Lattice, Phys. Rev. Lett. 97, 120402 (2006).
- [27] J. Amato-Grill, N. Jepsen, I. Dimitrova, W. Lunden, and W. Ketterle, Interaction spectroscopy of a twocomponent Mott insulator, Phys. Rev. A 99, 033612 (2019).
- [28] S. Will, T. Best, U. Schneider, L. Hackermüller, D.-S. Lühmann, and I. Bloch, Time-resolved observation of coherent multi-body interactions in quantum phase revivals, Nature 465, 197 (2010).
- [29] M. J. Mark, S. Flannigan, F. Meinert, J. P. D'Incao, A. J. Daley, and H.-C. Nägerl, Interplay between coherent and dissipative dynamics of bosonic doublons in an optical lattice, Phys. Rev. Res. 2, 043050 (2020).
- [30] V. Venu, P. Xu, M. Mamaev, F. Corapi, T. Bilitewski, J. P. D'Incao, C. J. Fujiwara, A. M. Rey, and J. H. Thywissen, Unitary p-wave interactions between fermions in an optical lattice, Nature 613, 262 (2023).
- [31] P. Xu, J. Yang, M. Liu, X. He, Y. Zeng, K. Wang, J. Wang, D. J. Papoular, G. V. Shlyapnikov, and M. Zhan, Interaction-induced decay of a heteronuclear two-atom system, Nature Communications 6, 7803 (2015).
- [32] J. D. Hood, Y. Yu, Y.-W. Lin, J. T. Zhang, K. Wang, L. R. Liu, B. Gao, and K.-K. Ni, Multichannel interactions of two atoms in an optical tweezer, Phys. Rev. Res. 2, 023108 (2020).
- [33] L. A. Reynolds, E. Schwartz, U. Ebling, M. Weyland, J. Brand, and M. F. Andersen, Direct measurements of collisional dynamics in cold atom triads, Phys. Rev. Lett. 124, 073401 (2020).
- [34] M. Lüscher, Volume dependence of the energy spectrum in massive quantum field theories: I. Stable particle states, Communications in Mathematical Physics 104, 177 (1986).
- [35] M. Lüscher, Volume dependence of the energy spectrum in massive quantum field theories: II. Scattering states, Communications in Mathematical Physics 105, 153 (1986).
- [36] L. Maiani and M. Testa, Final state interactions from euclidean correlation functions, Physics Letters B 245, 585 (1990).
- [37] L. Lellouch and M. Lüscher, Weak transition matrix elements from finite-volume correlation functions, Communications in Mathematical Physics 219, 31 (2001).
- [38] S. Beane, W. Detmold, K. Orginos, and M. Savage, Nuclear physics from lattice QCD, Progress in Particle and Nuclear Physics **66**, 1 (2011).
- [39] H.-W. Hammer, J.-Y. Pang, and A. Rusetsky, Threeparticle quantization condition in a finite volume: 2. general formalism and the analysis of data, Journal of High Energy Physics 2017, 115 (2017).
- [40] F. Müller and A. Rusetsky, On the three-particle analog of the Lellouch-Lüscher formula, Journal of High Energy Physics 2021, 152 (2021).
- [41] T. Kraemer, M. Mark, P. Waldburger, J. G. Danzl, C. Chin, B. Engeser, A. D. Lange, K. Pilch, A. Jaakkola, H. C. Nägerl, and R. Grimm, Evidence for Efimov quantum states in an ultracold gas of caesium atoms, Nature

- **440**, 315 (2006).
- [42] J. von Stecher, J. P. D'Incao, and C. H. Greene, Signatures of universal four-body phenomena and their relation to the Efimov effect, Nature Physics 5, 417 (2009).
- [43] F. Ferlaino, S. Knoop, M. Berninger, W. Harm, J. P. D'Incao, H.-C. Nägerl, and R. Grimm, Evidence for Universal Four-Body States Tied to an Efimov Trimer, Phys. Rev. Lett. 102, 140401 (2009).
- [44] A. Zenesini, B. Huang, M. Berninger, S. Besler, H.-C. Nägerl, F. Ferlaino, R. Grimm, C. H. Greene, and J. von Stecher, Resonant five-body recombination in an ultracold gas of bosonic atoms, New Journal of Physics 15, 043040 (2013).
- [45] G. Zürn, T. Lompe, A. N. Wenz, S. Jochim, P. S. Julienne, and J. M. Hutson, Precise Characterization of ⁶Li Feshbach Resonances Using Trap-Sideband-Resolved RF Spectroscopy of Weakly Bound Molecules, Phys. Rev. Lett. 110, 135301 (2013).
- [46] A. M. Kaufman, B. J. Lester, M. Foss-Feig, M. L. Wall, A. M. Rey, and C. A. Regal, Entangling two transportable neutral atoms via local spin exchange, Nature 527, 208 (2015).
- [47] A. L. Shaw, P. Scholl, R. Finkelstein, R. B.-S. Tsai, J. Choi, and M. Endres, Erasure cooling, control, and hyperentanglement of motion in optical tweezers, Science 388, 845 (2025), https://www.science.org/doi/pdf/10.1126/science.adn2618.
- [48] J. P. D'Incao, H. Suno, and B. D. Esry, Limits on universality in ultracold three-boson recombination, Phys. Rev. Lett. 93, 123201 (2004).
- [49] B. Huang, L. A. Sidorenkov, and R. Grimm, Finite-temperature effects on a triatomic Efimov resonance in ultracold cesium, Phys. Rev. A 91, 063622 (2015).
- [50] D. Blume, Few-body physics with ultracold atomic and molecular systems in traps, Reports on Progress in Physics 75, 046401 (2012).
- [51] A. G. Sykes, J. P. Corson, J. P. D'Incao, A. P. Koller, C. H. Greene, A. M. Rey, K. R. A. Hazzard, and J. L. Bohn, Quenching to unitarity: Quantum dynamics in a three-dimensional bose gas, Phys. Rev. A 89, 021601 (2014)
- [52] J. P. D'Incao, J. Wang, and V. E. Colussi, Efimov physics in quenched unitary bose gases, Phys. Rev. Lett. 121, 023401 (2018).
- [53] We note that while Γ_q is the exponential decay rate of an single quantum state, whereas in a bulk gas L_3 controls the rate of successive decays events, depleting the atom number and resulting in a non-exponential decay for the atomic density, n, according to: $dn/dt = -L_3n^3$.
- [54] H. Suno, B. D. Esry, C. H. Greene, and J. P. Burke, Three-body recombination of cold helium atoms, Phys. Rev. A 65, 042725 (2002).

- [55] J. Wang, J. P. D'Incao, and C. H. Greene, Numerical study of three-body recombination for systems with many bound states, Phys. Rev. A 84, 052721 (2011).
- [56] J.-L. Li, P. S. Julienne, J. Hecker Denschlag, and J. P. D'Incao, Spin hierarchy in van der Waals molecule formation via ultracold three-body recombination, Phys. Rev. A 111, 013308 (2025).
- [57] N. P. Mehta, S. T. Rittenhouse, J. P. D'Incao, J. von Stecher, and C. H. Greene, General theoretical description of n-body recombination, Phys. Rev. Lett. 103, 153201 (2009).
- [58] See Supplemental Material for additional details of our calculations, derivations and results, which includes Refs. [70–72].
- [59] J. P. D'Incao, Few-body physics in resonantly interacting ultracold quantum gases, Journal of Physics B: Atomic, Molecular and Optical Physics 51, 043001 (2018).
- [60] B. D. Esry, C. H. Greene, and H. Suno, Threshold laws for three-body recombination, Phys. Rev. A 65, 010705 (2001).
- [61] J. P. D'Incao and B. D. Esry, Scattering length scaling laws for ultracold three-body collisions, Phys. Rev. Lett. 94, 213201 (2005).
- [62] E. Nielsen, H. Suno, and B. D. Esry, Efimov resonances in atom-diatom scattering, Phys. Rev. A 66, 012705 (2002).
- [63] F. Werner and Y. Castin, Unitary quantum three-body problem in a harmonic trap, Phys. Rev. Lett. 97, 150401 (2006).
- [64] D. S. Petrov, C. Salomon, and G. V. Shlyapnikov, Weakly bound dimers of fermionic atoms, Phys. Rev. Lett. 93, 090404 (2004).
- [65] F. Werner and Y. Castin, Unitary gas in an isotropic harmonic trap: Symmetry properties and applications, Phys. Rev. A 74, 053604 (2006).
- [66] J.-L. Li, P. S. Julienne, J. Hecker Denschlag, and J. P. D'Incao, Spin structure of diatomic van der Waals molecules of alkali-metal atoms, Phys. Rev. A 111, 033302 (2025).
- [67] J. Wang, J. P. D'Incao, Y. Wang, and C. H. Greene, Universal three-body recombination via resonant d-wave interactions, Phys. Rev. A 86, 062511 (2012).
- [68] In ultracold quantum gases, the N-body loss rate coefficient, L_N , is defined such that the time evolution of atomic density, n, is given by: $dn/dt = -\sum_{N=2} L_N n^N$.
- [69] J. P. D'Incao and B. D. Esry, Manifestations of the Efimov effect for three identical bosons, Phys. Rev. A 72, 032710 (2005).
- [70] M. W. Jack, Decoherence due to Three-Body Loss and its Effect on the State of a Bose-Einstein Condensate, Phys. Rev. Lett. 89, 140402 (2002).
- [71] D. Rätzel and R. Schützhold, Decay of quantum sensitivity due to three-body loss in Bose-Einstein condensates, Phys. Rev. A 103, 063321 (2021).
- [72] W. Ham and K. Zhou, A short note on the volume of hypersphere (2006), arXiv:cs/0604056 [cs.IT].